Published in final edited form as:
Semin Perinatol. 2010 February ; 34(1): 46–56. doi:10.1053/j.semperi.2009.10.005.

Noninvasive Cerebral Perfusion Imaging in High-Risk Neonates

Donna A. Goff, MD, MS[*], **Erin M. Buckley, MS**[†], **Turgut Durduran, PhD**[†,‡,§], **Jiongjong Wang, PhD**[§], and **Daniel J. Licht, MD**[¶]

[*] Department of Cardiology, Children's Hospital of Philadelphia, Philadelphia, PA

[†] Department of Physics and Astronomy, University of Pennsylvania, Philadelphia, PA

[‡] Institut de Ciències Fotòniques, Castelldefels (Barcelona), Spain

[§] Department of Radiology, University of Pennsylvania, Philadelphia, PA

[¶] Department of Neurology, Children's Hospital of Philadelphia, Philadelphia, PA

Abstract

Advances in medical and surgical care of the high-risk neonate have led to increased survival. A significant number of these neonates suffer from neurodevelopmental delays and failure in school. The focus of clinical research has shifted to understanding events contributing to neurological morbidity in these patients. Assessing changes in cerebral oxygenation and regulation of cerebral blood flow (CBF) is important in evaluating the status of the central nervous system. Traditional CBF imaging methods fail for both ethical and logistical reasons. Optical near infrared spectroscopy (NIRS) is increasingly being used for bedside monitoring of cerebral oxygenation and blood volume in both very low birth weight infants and neonates with congenital heart disease. Although trends in CBF may be inferred from changes in cerebral oxygenation and/or blood volume, NIRS does not allow a direct measure of CBF in these populations. Two relatively new modalities, arterial spin-labeled perfusion magnetic resonance imaging and optical diffuse correlation spectroscopy, provide direct, noninvasive measures of cerebral perfusion suitable for the high-risk neonates. Herein we discuss the instrumentation, applications, and limitations of these noninvasive imaging techniques for measuring and/or monitoring CBF.

Keywords

infant cerebral blood flow; CBF; arterial spin labeled perfusion; MRI; PVL; optical spectroscopy

Advances in medical and surgical management have led to increase in survival among infants with severe conditions, including prematurity, birth trauma, and congenital malformations (congenital heart defects and congenital diaphragmatic hernia, among others). Minimizing factors that contribute to neurological morbidity prove to be a significant challenge facing physicians in the routine care of neonates with these conditions. Improving our ability to assess changes in cerebral oxygenation and regulation of cerebral blood flow (CBF) will enhance our

Address reprint requests to Daniel J. Licht, MD, Department of Neurology, Children's Hospital of Philadelphia, 34th and Civic Centre Blvd, Philadelphia, PA 19104. licht@email.chop.edu.

understanding of how these changes may contribute toward acquired brain injury in its various forms, including hypoxia-ischemic injury, periventricular leukomalacia (PVL), and perinatal stroke.

PVL is an ideal subject for research because large populations of infants are at risk and outcome studies have demonstrated a detrimental effect of PVL on function and quality of life.[1] Animal models of PVL exist and provide a rich background for mechanism of injury.[2,3] They also serve as subjects for investigating therapies for PVL protection and prevention. In human beings, premature delivery between 23 and 32 weeks is one of the strongest risk factors for PVL.[4–6] During this period, there is an increased vulnerability of the pre-myelinating oligodendrocyte precursors to injury.[2] In addition, several studies have shown that infants with complex congenital heart disease (CHD), such as hypoplastic left heart syndrome (HLHS) or d-transposition of the great arteries (d-TGA), are also at risk for PVL.[7–12] In both populations of at-risk newborns, hypoxia-ischemia, hypocarbia, and hypotension increase the risk of acquiring PVL.[4,5,13–17] In addition, the development of the circulatory system with an immature or absent cerebrovascular autoregulation may also play a significant role.[18,19]

The ability to regulate CBF begins in utero at an early gestation. Complex regulatory mechanisms maintain adequate blood flow and oxygenation to the fetal brain during growth and development.[20] Doppler velocimetry studies using umbilical artery (UA) and middle cerebral artery (MCA) pulsatility or resistance indexes demonstrate the ability of the fetus to autoregulate.[21] In a hypoxic environment, the fetus is able to “brain spare” by redistributing UA blood flow to the MCA, providing improved oxygenation to the brain.[22,23] Although a compensatory response exists, there is likely a threshold that once reached results in altered brain growth and development. Abnormal CBF dynamics have been observed in intrauterine growth restriction[22,24] and in fetuses with complex congenital heart lesions.[23,25] MCA pulsatility index, and resistance index are reduced in fetuses with HLHS and d-TGA compared with controls. These differences in cerebrovascular resistance in utero may alter brain development and autoregulatory capacity. Premature and/or very low birth weight (VLBW) infants may have delayed development of this autoregulatory system, increasing the risk of abnormal flow and oxygenation of the brain during periods of hemodynamic instability. Evidence demonstrates lower basal CBF[26] along with a compromised ability to regulate blood flow in the face of hemodynamic instability[10] in premature infants.

Recent preoperative magnetic resonance imaging (MRI) data from our group provide increasing evidence that brain maturation and growth is influenced by the in utero environment.[18] Term-gestation neonates with HLHS and d-TGA had smaller head circumferences and structurally immature brains compared with normal-term controls. These developmental abnormalities may increase the risk of impaired auto-regulatory abilities in infants with complex CHD, and this relationship is under active investigation. The ability to accurately measure CBF and/or changes in CBF in these high-risk neonates during periods of instability will lead to an increased understanding of risk for brain injury.

Very few modalities exist to monitor CBF in high-risk neonates. In the past 2 decades, near infrared spectroscopy (NIRS) has been the primary modality to assess *microvascular* cerebral oxygenation, inferring CBF from changes that occur in total hemoglobin concentration (or blood volume).[27] Although the use of NIRS has expanded in the clinical setting, most commercially available NIRS devices are limited to quantifying only relative changes in hemodynamic parameters.[28] Because they rely on a series of assumptions to derive CBF, they cannot provide direct quantitative measurements of CBF. Transcranial Doppler can be used to measure CBF velocity in the anterior, middle, and posterior cerebral arteries, but its use is limited only to short periods of assessment in neonates secondary to high-energy transmission over longer periods.[29] Recent advances in noninvasive imaging modalities, such as arterial

spin labeled perfusion magnetic resonance imaging (ASL-pMRI) and diffuse correlation spectroscopy (DCS), provide novel techniques for measurements of CBF in high-risk neonates. These newer modalities provide mechanisms to investigate changes in cerebral oxygen saturations and CBF to further elucidate factors that may contribute to development of brain injury.

Arterial Spin-Labeled Perfusion Magnetic Resonance Imaging

Until recently, dynamic susceptibility contrast approach has been the primary MRI modality to assess CBF. Its use in pediatrics has been limited by the need to use gadolinium contrast boluses, by the inability to make repeated measurements during a single session (secondary to cumulative effects), and by the lack of absolute quantification of blood flow.[30] A novel technique, ASL-pMRI, allows noninvasive evaluation of CBF using electromagnetically labeled arterial blood water as an endogenous contrast agent.[31] One of the most significant advantages of ASL-pMRI over previous techniques is the ability to assess CBF without using intravascular contrast agents or radioactive labeled tracers.

ASL-pMRI Technical

ASL-pMRI magnetically labels arterial blood by inversion or saturation proximal to the tissue of interest.[32] After a delay in time, image acquisition occurs allowing the labeled blood to flow into the imaging slices. Perfusion is determined by pair-wise comparison with separate images that are acquired without labeling (control). To improve the signal-to-noise ratio (SNR) of the perfusion images, repeated measurements of label and control are acquired over a period few minutes. Absolute CBF can be quantified in mL/100 g/min by taking into account the decay time of the electromagnetically labeled blood tracer T1.[31] There are 2 categories of ASL-pMRI: continuous ASL (CASL) and pulsed ASL (PASL). As demonstrated in Fig. 1, in CASL, continuous radio frequency (RF) is applied to the base of the brain for 1–2 seconds magnetically labeling blood flow traveling through this plane. In PASL, RF pulses with high peak amplitude but short duration (10–20 ms) are applied to a thick area of blood inferior to the imaging plane.

Measuring CBF with PASL in neonates and infants poses technical challenges related to their cerebrovascular physiology.[9,33] First, CBF in infants is lower than that of older children and adults. Second, blood T1 is relatively long.[34] These factors combined result in labeled blood contaminating the control images, culminating in a concentration of “negative voxels” on the final CBF map. The percentage of negative “voxels” increases as CBF decreases, and is the leading contributor to SNR.[35]

CASL provides a stronger perfusion contrast; however, it is more challenging to implement and deposits a higher level of RF power.[36] The long labeling pulses of the CASL scan can partially excite imaging slices through magnetization transfer and this needs to be balanced during control acquisition to quantify CBF accurately. One issue related to the use of CASL is that not all commercial MRI scanners allow long RF pulses for labeling (RF duty-cycle limit). Therefore, because of its technical simplicity and low RF power level, PASL has been used in investigation in neonates and children.

A newly developed labeling scheme termed pseudo-CASL or pulsed-CASL takes advantage of the higher labeling efficiency of CASL, while circumventing hardware limitations.[35,37] Pseudo-CASL uses a train of short RF pulses to mimic the effect of continuous spin labeling, providing improved labeling efficiency and compatibility with the standard body transmit coil and array receiver coils which are now widely used on commercial MRI systems. Experimental data in adults using pseudo-CASL showed a 50% increase of SNR compared with PASL, and a higher tagging efficiency than CASL (80% vs 68%). Computer simulations also predicted an optimal tagging efficiency of 85% for flow velocity from 10 to 60 cm/s.[35] Pseudo-CASL

is appealing for pediatric applications because it provides a well-defined labeling bolus (ie, the amount of arterial blood water flowing through the labeling plane during the tagging duration), with a relative stable tagging efficiency across a wide range of age populations.

To assess the performance of ASL-pMRI CBF imaging techniques in the pediatric population, we studied 10 children (age range, 4 days to 3 years) with CHD before and after hypercarbia, using a direct comparison of PASL and pseudo-CASL (Unpublished data, Licht). Figures 2 and 3 demonstrate direct comparisons of CBF measured by pseudo-CASL and PASL performed sequentially, whereas Fig. 4 compares the performance of these 2 techniques as measured by percent negative voxels seen in the imaging plane. On direct comparison, pseudo-CASL offers improvement in SNR and provides a more robust measure of CBF at low flows.

One of the primary limitations of ASL-perfusion imaging is that only a small volume of arterial blood (1%–2% of total brain volume) can be labeled and there is further relaxation during transit resulting in <1% of labeled blood reaching the region of brain tissue. Higher magnetic fields, such as 3.0-T can increase the SNR. Figure 5 compares performance of PASL CBF measurements at high (3.0 T) and low (1.5 T) field. In this study, neonates with CHD (3.0 T) were compared with a mixed population of infants and children (age range, 4 days to 3 years) at low field. The higher field improves SNR of PASL. However, with the increased SNR comes increased susceptibility effects (ie, shortened T2/T2*) that may cause underestimation of perfusion values, especially for CHD children with low arterial oxygen saturations.

Doppler ultrasound has shown that blood flow velocities in healthy children are higher than adults,[38] allowing a reduced transit time for labeled blood to flow from the labeling region to the brain. As a result, there is reduction in relaxation and transit effect as well as in focal intravascular signal in perfusion images. Data also suggest that children have an increased water content of the brain,[39] which results in increased equilibrium of MR signal, spin lattice, spin-spin relaxation (T1, T2), thus improving the signal through increased tracer and lifetime. Although ASL-pMRI can be used to measure CBF in neonates, it only provides a discrete time point and cannot be used at the bedside or in the operating room for longer periods of assessment.

ASL-pMRI in the High-Risk Neonate

High-risk neonates have inherently low CBF.[9,40,41] Imaging at high field (3.0 vs 1.5 T), reducing the labeling volume, and improving tagging efficiency (pseudo-CASL vs PASL) results in more reliable CBF maps by reducing the percentage negative voxels (SNR). Studies in normal neonates using ASL-pMRI have cataloged normal CBF in preterm- and term infants[33] as well as age related changes throughout childhood.[42] Other studies have demonstrated expected physiological responses; that CBF increases with lower hemoglobin and increases predictably with hypercarbia.[9] ASL-pMRI has also been useful in assessing CBF in neonates who have suffered hypoxia-ischemia[43] and in infants and children after stroke.[44]

Diffuse Optical Spectroscopies

Diffuse optical spectroscopies aim to investigate tissue physiology millimeters to centimeters below the tissue surface by using the spectral “window” of low absorption in the near-infrared range (NIR, 700–900 nm), as seen in Fig. 6.[45–47] In this range, scattering rather than absorption dominates photon transport, so that NIR light experiences thousands of scattering events and propagates centimeters into the tissue before it is either detected at the tissue surface or lost to absorption. The most commonly used diffuse optical technique, known as NIRS, measures slow variations in cerebral absorption and scattering and is thus sensitive to chromophore concentrations and therefore to cerebral oxygen saturation and cerebral blood volume (CBV).[48]

In additional, by monitoring the spatial and temporal changes in the speckle pattern of light interference on the tissue surface, we can infer information about tissue dynamics, because speckle fluctuations are caused by the motion of tissue scatterers, such as red blood cells.[49, 50] Most dynamic methods, such as laser Doppler flowmetry or laser speckle imaging, probe single light scattering events and thus only reach superficial tissue. However, our optical group at the University of Pennsylvania has pioneered a novel dynamic method, DCS, which works in the multiple scattering regime to probe the motion of red blood cells in deep tissue. The following sections will focus on these 2 methods (NIRS and DCS) and their applications in the high-risk neonate population.

Near-Infrared Spectroscopy

The attenuation of NIR light incident on tissue depends on both scattering and absorption, and it reveals information about the concentrations of tissue chromophores, such as oxy- and deoxyhemoglobin. NIRS measurements aim to recover the optical properties of tissue, namely the wavelength-dependent absorption and reduced scattering coefficients (cm^{-1}) (μ_a and μ_s, respectively) defined as the mean number of absorption and/or scattering events per unit length a photon travels, to extract tissue chromophore concentrations.[47] These concentrations are obtained using the following formula:

$$\mu_a(\lambda) = \sum_i C_i \varepsilon_i(\lambda) \tag{1}$$

where ε_i ($\mu M \times cm^{-1}$) is the known wavelength dependent extinction coefficient of the i^{th} chromophore. The 2 main endogenous absorbers in tissue in the NIR range are oxy- and deoxyhemoglobin, thus Equation 1 is typically written as $\mu_a(\lambda) = C_{Hb}\varepsilon_{Hb}(\lambda) + C_{HbO2}\varepsilon_{HbO2}(\lambda)$, where C_{Hb} and C_{HbO2} are the concentrations of tissue oxy- and deoxyhemoglobin, respectively. After μ_a is obtained at multiple wavelengths, quantifying hemoglobin concentrations simply requires solving a system of linear equations, that is, Equation 1 at multiple wavelengths.

Quantification of the wavelength-dependent tissue absorption and scattering coefficients requires a rigorous theoretic understanding of light transport in tissue. It is widely accepted that photon propagation over long distances through tissue is well approximated as a diffusive process, described by a photon diffusion equation.[47] This diffusion presents a stark contrast with other technologies, such as x-ray, in which photons travel straight through tissue. Using this diffusion model, tissue scattering may be separated from tissue absorption, and thus accurate calculations of tissue hemoglobin concentrations may be obtained.

As seen in Fig. 7, photon propagation through cortical tissue is most sensitive to hemodynamic perturbations within the darkest banana-shaped region (at a depth of approximately one-third to one-half the source-detector separation distance), with lighter regions having progressively less influence. This figure also demonstrates an important caveat of NIRS measurements: the thickness of skull, scalp, and cerebral spinal fluid layers may vary between subjects, thus affecting the resulting detected signal presumed to rise mainly from the cortical layers of the brain. Care must be taken during data analysis to account for the effects of the other layers through which light propagates before reaching cortical tissue.[51] The photon diffusion model, with the help of Monte Carlo simulations, can accurately account for the effects of tissue layers, such as skull, scalp, and cerebral spinal fluid.

NIRS Cerebral Hemodynamic Parameters of Interest—Studies conducted with NIRS on the high-risk neonate typically report absolute measures and/or relative changes of C_{Hb} (μM), C_{HbO2} (μM), total hemoglobin concentration (μM) (THC = $C_{Hb} + C_{HbO2}$), cerebral tissue

oxygen saturation (%) ($ScO_2 = C_{HbO2}/THC \times 100\%$), and/or hemoglobin difference (μM) ($HbD = C_{HbO2} - C_{Hb}$). From THC, CBV may be estimated by the following formula,

$$CBV = \frac{THC \times MW_{Hb}}{HGB \times R \times D_{bt} \times 10^5} \quad (2)$$

where MW_{Hb} = 64,500[g/moles] is the molecular weight of deoxyhemoglobin, HGB (g/dL) is the large vessel deoxyhemoglobin concentration, R is the large vessel-to-cerebral hematocrit ratio, and D_{bt} is the density of brain tissue (1.05 g/mL in neonates).[48] Typical commercially available NIRS devices do not provide the sophistication in instrumentation or data analysis to quantify absolute measures of these parameters (C_{Hb}, C_{HbO2}, THC, SCO_2, HbD, and CBV). Thus, many groups choose to report only relative changes in these parameters.

With the help of an exogenous tracer, such as oxygen or indocyanine green dye, NIRS may also quantify CBF (mL/min/100 g) using Equation 2.[52] This calculation of CBF relies on the Fick principle, which states that the total uptake of a tracer by tissue is proportional to the difference between the rates of inflow and outflow of the tracer to and from the tissue.

$$CBF = \frac{K \times \Delta C_{HbO2}}{tHb \int_0^t \Delta SaO_2 dt} \quad (3)$$

Here K is a constant reflecting cerebral to large vessel hematocrit ratio, molecular weight of hemoglobin, and cerebral tissue density; ΔC_{HbO2} is the change in cerebral oxyhemoglobin concentration measured by NIRS; tHb is the total arterial hemoglobin concentration determined from a blood sample; and ΔSaO_2 is the change in arterial oxygen saturation, determined from pulse-oximetry readings. This measurement provides a snapshot of regional tissue CBF in time; it does not provide continuous CBF data. Certain assumptions must be true for this method to be valid, namely that CBV, CBF, and cerebral oxygen extraction must remain constant. However, this technique has been validated with limited success.[53,54] The use of an exogenous tracer limits its use in the clinical setting, especially in high-risk neonates. Thus, NIRS reports of changes in CBF are typically inferences gathered from either changes in total hemoglobin concentration,[27] or from changes in the hemoglobin difference parameter.[55]

NIRS Instrumentation—As seen in Fig. 8A–C, there are 3 types of NIRS instruments.[56] Time-resolved NIRS (Fig. 8C) uses subnanosecond pulsed light to measure a histogram of photon arrival times of the reflected/transmitted diffuse light. This technique enables quantification of absolute optical properties using fits to the solution of the time-domain photon diffusion equation.[46] Thus, absolute measures of C_{Hb}, C_{HbO2}, THC, SCO_2 and CBV are feasible. With the high information content of time-resolved measurements comes a high cost of instrumentation components and complex data analysis.

Similar information, that is, absolute absorption and scattering coefficients that yield absolute measures of C_{Hb}, C_{HbO2}, THC, SCO_2 and CBV, can be obtained using a frequency domain (FD) NIRS instrument (Fig. 8B). In this configuration, NIR light is sinusoidally amplitude modulated at multiple frequencies in the MHz range.[57] More commonly, FD measurements are taken at a single frequency and absolute optical properties are derived from the FD photon diffusion equation with multiple source-detector separations.[58] The FD systems have the advantage of gathering similar information to the time domain systems, but the cost of sources and detectors, as well as the time for data acquisition and data analysis are significantly reduced.

Although the FD is not sensitive to stray room light, it can be sensitive to unwanted light that has leaked around the sample of interest and to surface coupling between the skin and optode.[56]

In studies for which absolute hemoglobin concentrations are less valuable than the relative changes in these concentrations, FD NIRS at a single source-detector separation or continuous wave (CW) NIRS (Fig. 8A) can be used. CW NIRS measures the attenuation of constant intensity source light after it has diffused through the tissue. Data are collected at multiple wavelengths, equal to or exceeding the number of chromophores measured.[59]

Commercially available NIRS instruments from companies, such as Hamamatsu, Somanetics, and NIRx Medical Technologies, are typically CW devices. Although the cost of a CW NIRS device is typically much less than that of a time domain or FD instrument, CW instruments are highly sensitive to room light, to surface coupling between skin and/or hair and the optical probe, and lead to crosstalk between calculated tissue absorption and scattering.[60,61] In addition, although reliable trends in hemodynamic changes may be obtained with these devices, accurate calculations of relative changes in chromophore concentrations may be highly influenced by the aforementioned factors.

Commercial system availability is crucial for wider use of NIRS in the clinic, and there are now even a handful of CW NIRS devices approved by the Food and Drug Administration.[28] The clinical utility of these devices remains to be determined by large clinical trials. Clinical researchers must be aware of the many limitations present in CW NIRS technology.

NIRS in the High-Risk Neonate—First described in 1985 for monitoring cerebral tissue oxygen saturations in preterm infants,[62] NIRS has slowly expanded to monitor high-risk neonates in a variety of clinical settings. In the high-risk neonatal brain, diffuse optical measurements are typically performed in a reflection geometry in which the light source(s) and detector(s) lie in the same plane. In a few studies, measurements have been made with sources and detectors widely spread across the infant's head to generate tomographic reconstructions.[63–65] At a given source-detector separation, NIR light penetrates deeper into the neonatal cortex compared with adult cortex because of the decreased thickness of the neonatal skull. Therefore, neonates are ideal candidates for NIRS monitoring. Conversely, NIRS is a particularly attractive tool for monitoring cerebral physiology in neonates because of its milliseconds temporal resolution, bedside capabilities, minimal deposition of energy, and its noninvasiveness.[66,67] Additionally, NIRS can easily be integrated with other monitoring techniques, such as MRI, Doppler ultrasound, electroencelography, or positron emission tomography. Unlike some of these other modalities, namely MRI and positron emission tomography, NIRS measurements are easily performed without the use of general anesthesia.

During the past decade, multiple investigations have used NIRS to evaluate cerebral oxygenation and blood flow in premature and/or VLBW infants[10,19] and in both the preoperative[68] and postoperative settings[69] of infants undergoing cardiac surgery.[7,10,70–72]

Premature and/or VLBW infants <30-week gestation exhibit perturbations in their transitional circulation.[73] In addition to immaturity of the myocardium and vasculature, persistent patency of ductus arteriosus and positive pressure ventilation contribute to alteration in postnatal physiology.[73] In preterm infants, mean arterial blood pressure has been used as an indicator of systemic cardiac output; the lower limit of normal being 30 mm Hg. In the clinical setting, a normal blood pressure measurement is assumed to equate with adequate cardiac output and adequate CBF. This assumption is challenged by Doppler echocardiographic studies measuring cardiac output and superior vena cava blood flow in preterm and term neonates, which suggests that blood pressure is not equivalent to systemic cardiac output and/or flow.[74,75] Because of

this limitation, NIRS has been used to assess changes in cerebral oxygenation in relation to blood pressure fluctuations in the high-risk neonate.

Passive cerebral perfusion, an indicator of failure of cerebral autoregulation, occurs when CBF changes are concordant with systemic blood pressure perturbations. In a NIRS study of premature infants (gestational age, 23–31 weeks), 17 of 32 (53%) infants had concordant changes in THC, presumed to be reflective of CBF, with changes in blood pressure. These changes provided evidence of passive cerebral perfusion.[69] In this same subgroup, 8 of 17 (47%) developed PVL.[76] In another study of premature infants weighing <1500 g, significant perturbations in hemodynamics and oxygenation were demonstrated to occur with complex care-giving and endotracheal tube repositioning.[10]

Investigations using NIRS have also increased in pediatric cardiology with a growing interest in understanding risks for perioperative brain injury. This has led to multiple studies evaluating the use of NIRS for noninvasive assessment of regional cerebral oxygen saturations before, during, and after congenital cardiac surgery.[70–72,77] However, there are limited data to suggest that this leads to improved neurological outcome.[78]

Brain injury in hypoxia-ischemia occurs as a result of cellular energy metabolism failure and expands as injured and dying cells release glutamate and calcium. Reperfusion brings oxygen to the injured tissue which increases concentrations of reactive oxygen species, thereby expanding the area of injury.[79,80] Although NIRS monitoring is not routinely used in this clinical setting, it may allow optimization of therapy by assessing changes in cerebral oxygenation during hypothermia or re-warming.

As outlined by Wolf et al,[28] there are many (approximately thousands of) commercial NIRS instruments in use, with a rapidly increasing number of studies being published. However, some of these studies were done without state-of-the-art instrumentation or algorithms, leading to debates over the utility of NIRS.[81–83] We believe that NIRS and related techniques offer a great deal of promise for cerebral monitoring in the high-risk neonate. With improvements in technology and in the physical understanding of the photon propagation through tissues, its utility is rapidly becoming clear.

Diffuse Correlation Spectroscopy

DCS, originally dubbed diffusing wave spectroscopy,[84,85] uses NIR light to probe the dynamics of deep tissues. DCS continuously monitors relative changes in microvascular CBF (absolute calculations have not been quantified to date)[86–94] as opposed to NIRS that monitors cerebral blood oxygen saturation and volume. DCS measures of relative blood flow have been extensively validated as a using comparisons to literature,[88,95–97] to Doppler ultrasound in murine tumors and in the preterm infant brain,[98,99] to laser Doppler flowmetry in rat brain,[89,94,96] to fluorescent microspheres in piglet brains[93] and to arterial spin-labeled perfusion MRI in human brain.[97] It has also been used to measure blood flow in many organs, including brain, muscle, and breast.[100–105] DCS is a novel technique, and, to the best of our knowledge, only 3 groups have published peer-reviewed works on DCS to date.[91,92,106,107] DCS is being adapted by numerous other groups and we expect that its use will grow rapidly in the upcoming decade.

In DCS, coherent NIR light, that is, light that is spatially in phase over long distance, is introduced into tissue wherein it travels deeply and elastically scatters thousands of times before detection at some distance from the light source. Each scattering event alters the phase of the scattered light. At the detector, the superposition of multiple light fields with different phases creates a speckle pattern of interference. If the scattering particles are in motion, the speckle pattern fluctuates in time. Fluctuations of the speckle pattern thus contain information

about the motion of the scatterers.[84,85] In tissue, the primary moving scatterers are red blood cells.[50] Therefore, by characterizing the fluctuations in speckle intensity over time using an intensity autocorrelation function, we gather information about blood flow in tissue (see Fig. 9A for a typical intensity autocorrelation function gathered on a neonate with HLHS).

Diffuse Correlation Spectroscopy Instrumentation—The DCS instrument uses a low power (<50 mW), long-coherence-length laser operating in the NIR range to deliver light to the tissue. Typically, single or few mode detection fibers are secured at a fixed distance from the source (Fig. 7). An intensity autocorrelation function is calculated based on photon arrival times at the detector location.[108] Blood flow dictates the decay rate of this autocorrelation function (see Fig. 9A), that is, the faster the curve decays, the faster the motion of the red blood cells. Figure 9A demonstrates this point with a hypercapnia experiment on a patient with HLHS.[109] The probe was placed on the patient's forehead (similar to Fig. 7), and DCS was used to monitor changes in CBF for a 5-minute baseline period of room air inhalation, followed by a 30-minute period of hypercapnia. Two sample autocorrelation curves from this experiment are displayed in Fig. 9A. As expected, the sample curve recorded during the baseline decays much slower than the sample curve obtained during hypercapnia, indicating an increase in blood flow during the hypercapnia.

A blood flow index (BFI) with units of cm^2/s, is defined to quantify the decay rate of the autocorrelation curves. BFI reflects CBF, and changes in BFI relative to baseline measurements reflect analogous changes in CBF. Figure 9B shows the time course of relative changes in CBF (rCBF) calculated from changes in the blood flow index measured during the earlier described hypercapnia experiment. As mentioned earlier in the text, although this analysis is empirical, it has been extensively validated. Improved physical modeling is in process to obtain absolute measurements of CBF.

DCS in the High-Risk Neonate—DCS is ideal for the high-risk neonate population, as it can be used as a continuous, noninvasive, low-risk, readily portable bedside monitor of relative changes in regional cortical CBF. Additionally, DCS can easily be combined with other modalities, such as NIRS, Doppler ultrasound, or electroencelography, to enhance the information gathered about the patient's physiology. Few studies have been conducted with DCS on this population, largely because of the newness of the technology. Buckley et al[98] have used DCS to monitor cerebral hemodynamics in VLBW preterm infants during a small postural change. Zhou et al[93] used a hybrid NIRS/DCS instrument to study the after effects of traumatic brain injury on the hemodynamics of the neonatal piglet cortex. Significant increases in total hemoglobin concentration were observed compared with preinjury levels, whereas cerebral oxygen saturation and rCBF immediately dropped significantly postinjury.

Thus, this preliminary data suggest that DCS can be a valuable tool to monitor relative changes in regional cerebral hemodynamics in high-risk neonates. Ideally, a study would use a hybrid NIRS and/or DCS instrument[86,94,96,97,110] to capture both tissue oxygenation and blood flow changes. These 2 parameters combined would further enable construction of indexes for measuring cerebral metabolic rate of oxygen extraction ($CMRO_2$).[96,97]

Summary

Over the past few decades, significant advances have been made in improving the survival of premature or VLBW neonates and neonates with CHD. With these advances in medical and surgical therapy, clinicians are now focusing their attention on reducing the morbidity associated with routine neonatal care. A major area of focus has been the greater understanding of the factors that contribute to impaired neurological development. Currently, NIRS has been the modality used to monitor changes in cerebral oxygenation. NIRS has provided very

important insight into cerebral oxygenation during routine care[10] and before, during, and after infant heart surgery.[68,70–72,77] Recent advances in novel research imaging modalities like ASL-pMRI and DCS will allow us to increase our understanding of basic cerebrovascular physiology and changes that occur in at-risk populations of infants, including premature infants, neonates with congenital heart defects, and neonates with other pathologic states, such as in hypoxia-ischemic injury and stroke. Increasing our understanding of regulation of CBF and the perturbations that occur during injury will allow us to further investigate the factors that contribute to central nervous system injury.

Acknowledgments

Dr. Goff is supported by an NHLBI grant number T32 HL-07915.

Dr. Durduran and Ms. Buckley are supported in part by the Thrasher Foundation, grant number NR 0016.

Dr. Wang is supported in part by MH080892, RR02305, and by the Thrasher Foundation.

Dr. Licht is supported in part by NINDS K-23 NS-052380, by the Steve and June Wolfson Fund for Neurological Research, and by the DANA Foundation.

References

1. Mathur A, Inder T. Magnetic resonance imaging—insights into brain injury and outcomes in premature infants. J Commun Disord 2009;42:248–255. [PubMed: 19406431]
2. Back SA, Han BH, Luo NL, et al. Selective vulnerability of late oligodendrocyte progenitors to hypoxia-ischemia. J Neurosci 2002;22:455–463. [PubMed: 11784790]
3. Drobyshevsky A, Song SK, Gamkrelidze G, et al. Developmental changes in diffusion anisotropy coincide with immature oligodendrocyte progression and maturation of compound action potential. J Neurosci 2005;25:5988–5997. [PubMed: 15976088]
4. Back SA, Riddle A, McClure MM. Maturation-dependent vulnerability of perinatal white matter in premature birth. Stroke 2007;38:724–730. [PubMed: 17261726]
5. Rezaie P, Dean A. Periventricular leukomalacia, inflammation and white matter lesions within the developing nervous system. Neuropathology 2002;22:106–132. [PubMed: 12416551]
6. Valcamonico A, Accorsi P, Sanzeni C, et al. Mid- and long-term outcome of extremely low birthweight (ELBW) infants: an analysis of prognostic factors. J Matern Fetal Neonatal Med 2007;20:465–471. [PubMed: 17674256]
7. Du Plessis AJ. Near-infrared spectroscopy for the in vivo study of cerebral hemodynamics and oxygenation. Curr Opin Pediatr 1995;7:632–639. [PubMed: 8776012]
8. Du Plessis AJ. Cerebrovascular injury in premature infants: current understanding and challenges for future prevention. Clin Perinatol 2008;35:609–641. [PubMed: 19026331]
9. Licht DJ, Wang J, Silvestre DW, et al. Preoperative cerebral blood flow is diminished in neonates with severe congenital heart defects. J Thorac Cardiovasc Surg 2004;128:841–849. [PubMed: 15573068]
10. Limperopoulos C, Gauvreau KK, O'Leary H, et al. Cerebral hemodynamic changes during intensive care of preterm infants. Pediatrics 2008;122:e1006–e1013. [PubMed: 18931348]
11. Miller SP, McQuillen PS, Vigneron DB, et al. Preoperative brain injury in newborns with transposition of the great arteries. Ann Thorac Surg 2004;77:1698–1706. [PubMed: 15111170]
12. Petit CJ, Rome JJ, Wernovsky G, et al. Preoperative brain injury in transposition of the great arteries is associated with oxygenation and time to surgery, not balloon atrial septostomy. Circulation 2009;119:709–716. [PubMed: 19171858]
13. Back SA. Perinatal white matter injury: the changing spectrum of pathology and emerging insights into pathogenetic mechanisms. Ment Retard Dev Disabil Res Rev 2006;12:129–140. [PubMed: 16807910]
14. Back SA, Rivkees SA. Emerging concepts in periventricular white matter injury. Semin Perinatol 2004;28:405–414. [PubMed: 15693397]

15. Galli KK, Zimmerman RA, Jarvik GP, et al. Periventricular leukomalacia is common after neonatal cardiac surgery. J Thorac Cardiovasc Surg 2004;127:692–704. [PubMed: 15001897]
16. Giannakopoulou C, Korakaki E, Manoura A, et al. Significance of hypocarbia in the development of periventricular leukomalacia in preterm infants. Pediatr Int 2004;46:268–273. [PubMed: 15151541]
17. Volpe, JJ. Hypoxic-ischemic encephalopathy: neuropathology and pathogenesis. In: Volpe, JJ., editor. Neurology of the Newborn. 5. Philadelphia: Saunders Elsevier; 2008.
18. Licht DJ, Shera DM, Clancy RR, et al. Brain maturation is delayed in infants with complex congenital heart defects. J Thorac Cardiovasc Surg 2009;137:529–536. [PubMed: 19258059]
19. Soul JS, Hammer PE, Tsuji M, et al. Fluctuating pressure-passivity is common in the cerebral circulation of sick premature infants. Pediatr Res 2007;61:467–473. [PubMed: 17515873]
20. Greisen G. Effect of cerebral blood flow and cerebrovascular autoregulation on the distribution, type and extent of cerebral injury. Brain Pathol 1992;2:223–228. [PubMed: 1343837]
21. Abuhamad, AZ. The role of Doppler ultrasound in obstetrics. In: Callen, PW., editor. Ultrasonography in Obstetrics and Gynecology. Philadelphia: Saunders Elsevier; 2008. p. 794-807.
22. Degani S, Lewinsky RM, Shapiro I. Doppler studies of fetal cerebral blood flow. Ultrasound Obstet Gynecol 1994;4:158–165. [PubMed: 12797213]
23. Donofrio MT, Bremer YA, Schieken RM, et al. Autoregulation of cerebral blood flow in fetuses with congenital heart disease: the brain sparing effect. Pediatr Cardiol 2003;24:436–443. [PubMed: 14627309]
24. Degani S. Fetal cerebrovascular circulation: a review of prenatal ultrasound assessment. Gynecol Obstet Invest 2008;66:184–196. [PubMed: 18607112]
25. Kaltman JR, Di H, Tian Z, et al. Impact of congenital heart disease on cerebrovascular blood flow dynamics in the fetus. Ultrasound Obstet Gynecol 2005;25:32–36. [PubMed: 15593334]
26. Yoxall CW, Weindling AM. Measurement of cerebral oxygen consumption in the human neonate using near infrared spectroscopy: cerebral oxygen consumption increases with advancing gestational age. Pediatr Res 1998;44:283–290. [PubMed: 9727702]
27. Grubb RL Jr, Raichle ME, Eichling JO, et al. The effects of changes in $PaCO_2$ on cerebral blood volume, blood flow, and vascular mean transit time. Stroke 1974;5:630–639. [PubMed: 4472361]
28. Wolf M, Ferrari M, Quaresima V. Progress of near-infrared spectroscopy and topography for brain and muscle clinical applications. J Biomed Opt 2007;12:14.
29. Ipsiroglu OS, Steck J, Michel E, et al. Are adult transcranial Doppler systems suitable for application in neonates? Eur J Pediatr 1996;155:942–947. [PubMed: 8911894]
30. Cha S. Dynamic susceptibility-weighted contrast-enhanced perfusion MR imaging in pediatric patients. Neuroimaging Clin N Am 2006;16:137–147. ix. [PubMed: 16543089]
31. Wang J, Licht DJ, Jahng GH, et al. Pediatric perfusion imaging using pulsed arterial spin labeling. J Magn Reson Imaging 2003;18:404–413. [PubMed: 14508776]
32. Detre JA, Alsop DC. Perfusion magnetic resonance imaging with continuous arterial spin labeling: methods and clinical applications in the central nervous system. Eur J Radiol 1999;30:115–124. [PubMed: 10401592]
33. Miranda MJ, Olofsson K, Sidaros K. Noninvasive measurements of regional cerebral perfusion in preterm and term neonates by magnetic resonance arterial spin labeling. Pediatr Res 2006;60:359–363. [PubMed: 16857776]
34. Wang J, Licht DJ. Pediatric perfusion MR imaging using arterial spin labeling. Neuroimaging Clin N Am 2006;16:149–167. ix. [PubMed: 16543090]
35. Wu WC, Wong EC. Feasibility of velocity selective arterial spin labeling in functional MRI. J Cereb Blood Flow Metab 2007;27:831–838. [PubMed: 16926843]
36. Wang J, Zhang Y, Wolf RL, et al. Amplitude-modulated continuous arterial spin-labeling 3.0-T perfusion MR imaging with a single coil: feasibility study. Radiology 2005;235:218–228. [PubMed: 15716390]
37. Dai W, Carmichael OT, Lopez OL, et al. Effects of image normalization on the statistical analysis of perfusion MRI in elderly brains. J Magn Reson Imaging 2008;28:1351–1360. [PubMed: 19025942]
38. Schoning M, Buchholz R, Walter J. Comparative study of transcranial color duplex sonography and transcranial Doppler sonography in adults. J Neurosurg 1993;78:776–784. [PubMed: 8468608]

39. Dobbing J, Sands J. Quantitative growth and development of human brain. Arch Dis Child 1973;48:757–767. [PubMed: 4796010]
40. Greeley WJ, Ungerleider RM, Kern FH, et al. Effects of cardiopulmonary bypass on cerebral blood flow in neonates, infants, and children. Circulation 1989;80:I209–I215. [PubMed: 2766529]
41. Pryds O, Greisen G. Effect of $PaCO_2$ and haemoglobin concentration on day to day variation of CBF in preterm neonates. Acta Paediatr Scand 1989;360(Suppl):33–36.
42. Biagi L, Abbruzzese A, Bianchi MC, et al. Age dependence of cerebral perfusion assessed by magnetic resonance continuous arterial spin labeling. J Magn Reson Imaging 2007;25:696–702. [PubMed: 17279531]
43. Pollock JM, Whitlow CT, Deibler AR, et al. Anoxic injury-associated cerebral hyperperfusion identified with arterial spin-labeled MR imaging. AJNR Am J Neuroradiol 2008;29:1302–1307. [PubMed: 18451089]
44. Chen J, Licht DJ, Smith SE, et al. Arterial spin labeling perfusion MRI in pediatric arterial ischemic stroke: initial experiences. J Magn Reson Imaging 2009;29:282–290. [PubMed: 19161176]
45. Jobsis FF. Noninvasive, infrared monitoring of cerebral and myocardial oxygen sufficiency and circulatory parameters. Science 1977;198:1264–1267. [PubMed: 929199]
46. Patterson MS, Chance B, Wilson BC. Time resolved reflectance and transmittance for the noninvasive measurement of tissue optical properties. Appl Opt 1989;28:2331–2336.
47. Yodh AG, Chance B. Spectroscopy and imaging with diffusing light. Phys Today 1995:34–40.
48. Wyatt JS, Cope M, Delpy DT, et al. Quantification of cerebral oxygenation and haemodynamics in sick newborn infants by near infrared spectrophotometry. Lancet 1986;2:1063–1066. [PubMed: 2877225]
49. Bonner R, Nossal R. Model for laser Doppler measurements of blood flow in tissue. Appl Opt 1981;20:2097–2107.
50. Cope, M. PhD Thesis. London: University of London; 1991. The Application of near Infrared Spectroscopy to Noninvasive Monitoring of Cerebral Oxygenation in the Newborn Infant.
51. Okada E, Delpy DT. Near-infrared light propagation in an adult head model. I. Modeling of low-level scattering in the cerebrospinal fluid layer. Appl Opt 2003;42:2906–2914. [PubMed: 12790439]
52. Edwards AD, Wyatt JS, Richardson C, et al. Cotside measurement of cerebral blood flow in ill newborn infants by near infrared spectroscopy. Lancet 1988;2:770–771. [PubMed: 2901613]
53. Brown DW, Picot PA, Naeini JG, et al. Quantitative near infrared spectroscopy measurement of cerebral hemodynamics in newborn piglets. Pediatr Res 2002;51:564–570. [PubMed: 11978878]
54. Schytz HW, Wienecke T, Jensen LT, et al. Changes in cerebral blood flow after acetazolamide: an experimental study comparing near-infrared spectroscopy and SPECT. Eur J Neurol 2009;16:461–467. [PubMed: 19236469]
55. Soul JS, Taylor GA, Wypij D, et al. Noninvasive detection of changes in cerebral blood flow by near-infrared spectroscopy in a piglet model of hydrocephalus. Pediatr Res 2000;48:445–449. [PubMed: 11004233]
56. Gibson AP, Hebden JC, Arridge SR. Recent advances in diffuse optical imaging. Phys Med Biol 2005;50:R1–R43. [PubMed: 15773619]
57. Pham TH, Coquoz O, Fishkin JB, et al. Broad bandwidth frequency domain instrument for quantitative tissue optical spectroscopy. Rev Sci Instrum 2000;71:2500–2513.
58. Fishkin JB, Gratton E. Propagation of photon-density waves in strongly scattering media containing an absorbing semi-infinite plane bounded by a straight edge. J Opt Soc Am A 1993;10:127–140. [PubMed: 8478741]
59. Duncan A, Meek JH, Clemence M, et al. Optical pathlength measurements on adult head, calf and forearm and the head of the newborn infant using phase resolved optical spectroscopy. Phys Med Biol 1995;40:295–304. [PubMed: 7708855]
60. Arridge SR, Lionheart WR. Nonuniqueness in diffusion-based optical tomography. Opt Lett 1998;23:882–884. [PubMed: 18087373]
61. Corlu A, Choe R, Durduran T, et al. Diffuse optical tomography with spectral constraints and wavelength optimization. Applied Optics 2005;44:2082–2093. [PubMed: 15835357]

62. Brazy JE, Lewis DV, Mitnick MH, et al. Noninvasive monitoring of cerebral oxygenation in preterm infants: preliminary observations. Pediatrics 1985;75:217–225. [PubMed: 2982128]
63. Austin T, Gibson AP, Branco G, et al. Three dimensional optical imaging of blood volume and oxygenation in the neonatal brain. Neuroimage 2006;31:1426–1433. [PubMed: 16644237]
64. Gibson AP, Austin T, Everdell NL, et al. Three-dimensional whole-head optical tomography of passive motor evoked responses in the neonate. Neuroimage 2006;30:521–528. [PubMed: 16246586]
65. Hebden JC, Gibson A, Yusof RM, et al. Three-dimensional optical tomography of the premature infant brain. Phys Med Biol 2002;47:4155–4166. [PubMed: 12502040]
66. Soul JS, du Plessis AJ. New technologies in pediatric neurology. Near-infrared spectroscopy. Semin Pediatr Neurol 1999;6:101–110. [PubMed: 10404564]
67. van Bel F, Lemmers P, Naulaers G. Monitoring neonatal regional cerebral oxygen saturation in clinical practice: value and pitfalls. Neonatology 2008;94:237–244. [PubMed: 18784420]
68. Johnson BA, Hoffman GM, Tweddell JS, et al. Near-infrared spectroscopy in neonates before palliation of hypoplastic left heart syndrome. Ann Thorac Surg 2009;87:571–577. [PubMed: 19161781]
69. Bassan H, Gauvreau K, Newburger JW, et al. Identification of pressure passive cerebral perfusion and its mediators after infant cardiac surgery. Pediatr Res 2005;57:35–41. [PubMed: 15531739]
70. Du Plessis AJ. Cerebral hemodynamics and metabolism during infant cardiac surgery. Mechanisms of injury and strategies for protection. J Child Neurol 1997;12:285–300. [PubMed: 9378896]
71. Ghanayem NS, Mitchell ME, Tweddell JS, et al. Monitoring the brain before, during, and after cardiac surgery to improve long-term neurodevelopmental outcomes. Cardiol Young 2006;16(suppl 3):103–109. [PubMed: 17378048]
72. Hoffman GM, Stuth EA, Jaquiss RD, et al. Changes in cerebral and somatic oxygenation during stage 1 palliation of hypoplastic left heart syndrome using continuous regional cerebral perfusion. J Thorac Cardiovasc Surg 2004;127:223–233. [PubMed: 14752434]
73. Kluckow M. Low systemic blood flow and pathophysiology of the preterm transitional circulation. Early Hum Dev 2005;81:429–437. [PubMed: 15935920]
74. Kluckow M, Evans N. Relationship between blood pressure and cardiac output in preterm infants requiring mechanical ventilation. J Pediatr 1996;129:506–512. [PubMed: 8859256]
75. Kluckow M, Evans N. Superior vena cava flow in newborn infants: a novel marker of systemic blood flow. Arch Dis Child Fetal Neonatal Ed 2000;82:F182–F187. [PubMed: 10794783]
76. Tsuji M, Saul JP, du Plessis A, et al. Cerebral intravascular oxygenation correlates with mean arterial pressure in critically ill premature infants. Pediatrics 2000;106:625–632. [PubMed: 11015501]
77. Du Plessis AJ, Newburger J, Jonas RA, et al. Cerebral oxygen supply and utilization during infant cardiac surgery. Ann Neurol 1995;37:488–497. [PubMed: 7717685]
78. Hirsch JC, Charpie JR, Ohye RG, et al. Near-infrared spectroscopy: what we know and what we need to know—a systematic review of the congenital heart disease literature. J Thorac Cardiovasc Surg 2009;137:154–112. [PubMed: 19154918]
79. Laptook AR. Use of therapeutic hypothermia for term infants with hypoxic-ischemic encephalopathy. Pediatr Clin N Am 2009;56:601–616. Table.
80. Sahni R, Sanocka UM. Hypothermia for hypoxic-ischemic encephalopathy. Clin Perinatol 2008;35:717–734. vi. [PubMed: 19026336]
81. Gomersall CD, Joynt GM, Gin T, et al. Failure of the INVOS 3100 cerebral oximeter to detect complete absence of cerebral blood flow. Crit Care Med 1997;25:1252–1254. [PubMed: 9233756]
82. Nicklin SE, Hassan IA, Wickramasinghe YA, et al. The light still shines, but not that brightly? The current status of perinatal near infrared spectroscopy. Arch Dis Child Fetal Neonatal Ed 2003;88:F263–F268. [PubMed: 12819155]
83. Schwarz G, Litscher G, Kleinert R, et al. Cerebral oximetry in dead subjects. J Neurosurg Anesthesiol 1996;8:189–193. [PubMed: 8803829]
84. Maret G, Wolf P. Multiple light scattering from disordered media. The effect of Brownian motion of scatterers. Z Physik B Condens Matters 1987;65:409–413.
85. Pine DJ, Weitz DA, Chaikin PM, et al. Diffusing wave spectroscopy. Phys Rev Lett 1988;60:1134–1137. [PubMed: 10037950]

86. Cheung C, Culver JP, Takahashi K, et al. In vivo cerebrovascular measurement combining diffuse near-infrared absorption and correlation spectroscopies. Phys Med Biol 2001;46:2053–2065. [PubMed: 11512610]
87. Culver JP, Durduran T, Cheung C, et al. Diffuse optical measurement of hemoglobin and cerebral blood flow in rat brain during hypercapnia, hypoxia and cardiac arrest. Adv Exp Med Biol 2003;510:293–297. [PubMed: 12580443]
88. Durduran, T. PhD dissertation. University of Pennsylvania; 2004. Non-Invasive Measurements of Tissue Hemodynamics with Hybrid Diffuse Optical Methods.
89. Durduran T, Yu G, Burnett MG, et al. Diffuse optical measurement of blood flow, blood oxygenation, and metabolism in a human brain during sensorimotor cortex activation. Opt Lett 2004;29:1766–1768. [PubMed: 15352363]
90. Durduran T, Zhou C, Edlow BL, et al. Transcranial optical monitoring of cerebrovascular hemodynamics in acute stroke patients. Opt Express 2009;17:3884–3902. [PubMed: 19259230]
91. Jaillon F, Li J, Dietsche G, et al. Activity of the human visual cortex measured non-invasively by diffusing-wave spectroscopy. Opt Express 2007;15:6643–6650. [PubMed: 19546974]
92. Li J, Ninck M, Koban L, et al. Transient functional blood flow change in the human brain measured noninvasively by diffusing-wave spectroscopy. Opt Lett 2008;33:2233–2235. [PubMed: 18830362]
93. Zhou C, Eucker SA, Durduran T, et al. Diffuse optical monitoring of hemodynamic changes in piglet brain with closed head injury. J Biomed Opt 2009;14:034015. [PubMed: 19566308]
94. Zhou C, Yu G, Daisuke F, et al. Diffuse optical correlation tomography of cerebral blood flow during cortical spreading depression in rat brain. Opt Express 2006;14:1125–1144. [PubMed: 19503435]
95. Cheung R, Solonenko M, Busch TM, et al. Correlation of in vivo photosensitizer fluorescence and photodynamic-therapy-induced depth of necrosis in a murine tumor model. J Biomed Opt 2003;8:248–252. [PubMed: 12683850]
96. Culver JP, Durduran T, Furuya T, et al. Diffuse optical tomography of cerebral blood flow, oxygenation, and metabolism in rat during focal ischemia. J Cereb Blood Flow Metab 2003;23:911–924. [PubMed: 12902835]
97. Durduran T, Yu G, Burnett MG, et al. Diffuse optical measurement of blood flow, blood oxygenation, and metabolism in a human brain during sensorimotor cortex activation. Opt Lett 2004;29:1766–1768. [PubMed: 15352363]
98. Buckley EM, Cook NM, Durduran T, et al. Cerebral hemodynamics in preterm infants during positional intervention measured with diffuse correlation spectroscopy and transcranial Doppler ultrasound. Opt Express 2009;17:12571–12581. [PubMed: 19654660]
99. Yu GQ, Durduran T, Zhou C, et al. Noninvasive monitoring of murine tumor blood flow during and after photodynamic therapy provides early assessment of therapeutic efficacy. Clin Cancer Res 2005;11:3543–3552. [PubMed: 15867258]
100. Durduran T, Choe R, Yu GQ, et al. Diffuse optical measurement of blood flow in breast tumors. Opt Lett 2005;30:2915–2917. [PubMed: 16279468]
101. Sunar U, Quon H, Durduran T, et al. Noninvasive diffuse optical measurement of blood flow and blood oxygenation for monitoring radiation therapy in patients with head and neck tumors: a pilot study. J Biomed Opt 2006;11:064, 021.
102. Yu G, Durduran T, Zhou C, et al. Real-time in Situ monitoring of human prostate photodynamic therapy with diffuse light. Photochem Photobiol 2006;82:1279–1284. [PubMed: 16696593]
103. Yu G, Floyd TF, Durduran T, et al. Validation of diffuse correlation spectroscopy for muscle blood flow with concurrent arterial spin labeled perfusion MRI. Opt Express 2007;15:1064–1075. [PubMed: 19532334]
104. Yu GQ, Durduran T, Lech G, et al. Time-dependent blood flow and oxygenation in human skeletal muscles measured with noninvasive near-infrared diffuse optical spectroscopies. J Biomed Opt 2005;10:024027024,021–024,012.
105. Zhou C, Choe R, Shah N, et al. Diffuse optical monitoring of blood flow and oxygenation in human breast cancer during early stages of neoadjuvant chemotherapy. J Biomed Opt 2007;12:051903. [PubMed: 17994886]

106. Dietsche G, Ninck M, Ortolf C, et al. Fiber-based multispeckle detection for time-resolved diffusing-wave spectroscopy: characterization and application to blood flow detection in deep tissue. Appl Opt 2007;46:8506–8514. [PubMed: 18071383]

107. Li J, Dietsche G, Iftime D, et al. Noninvasive detection of functional brain activity with near-infrared diffusing-wave spectroscopy. J Biomed Opt 2005;10

108. Brown, W., editor. Dynamic Light Scattering: The Method and Some Applications. Oxford, UK: Oxford University Press; 1993.

109. Durduran T, Zhou C, Kim MN, et al. Validation of diffuse correlation spectroscopy for non-invasive, continuous monitoring of CBF in neonates with congenital heart defects. Ann Neurol 2008;64:S63.

110. Durduran T. Noninvasive measurements of tissue hemodynamics with hybrid diffuse optical methods. Med Phys 2004;31:2178.

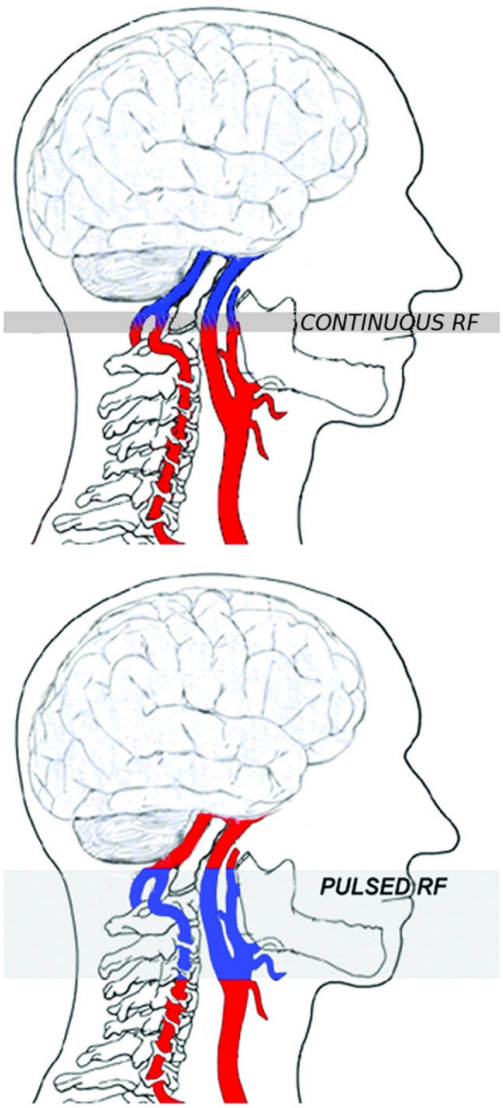

Figure 1.
Labeling planes for continuous ASL (CASL) vs pulsed ASL (PASL). In CASL, continuous radio frequency (RF) is applied to the base of the brain for 1–2 seconds, magnetically labeling blood flow traveling through the plane. In PASL, RF pulses with high peak amplitude but short duration (10–20 ms) are applied to a thick area of blood inferior to the imaging plane. (Color version of figure is available online.)

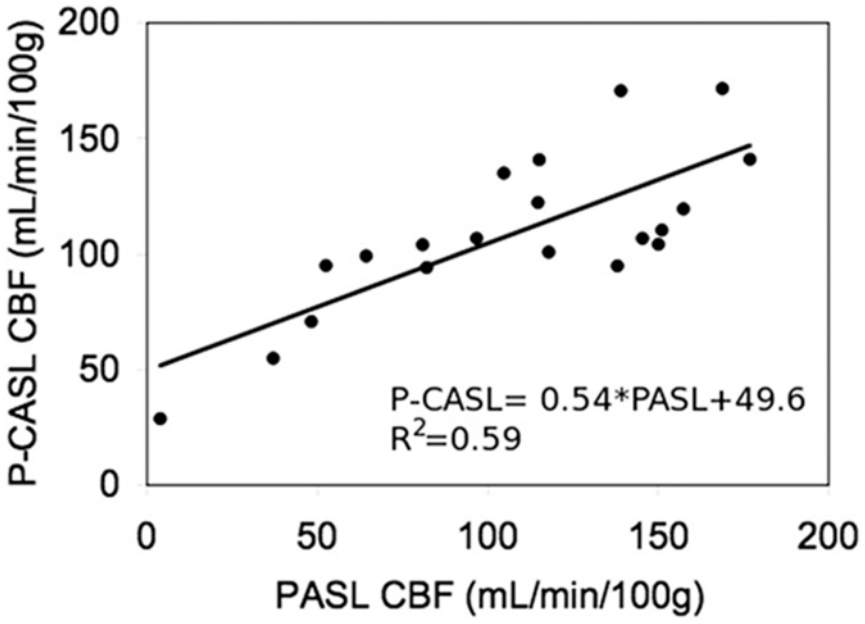

Figure 2.
Direct comparison of mean whole brain CBF as measured by PCASL (y-axis) and PASL (x-axis).

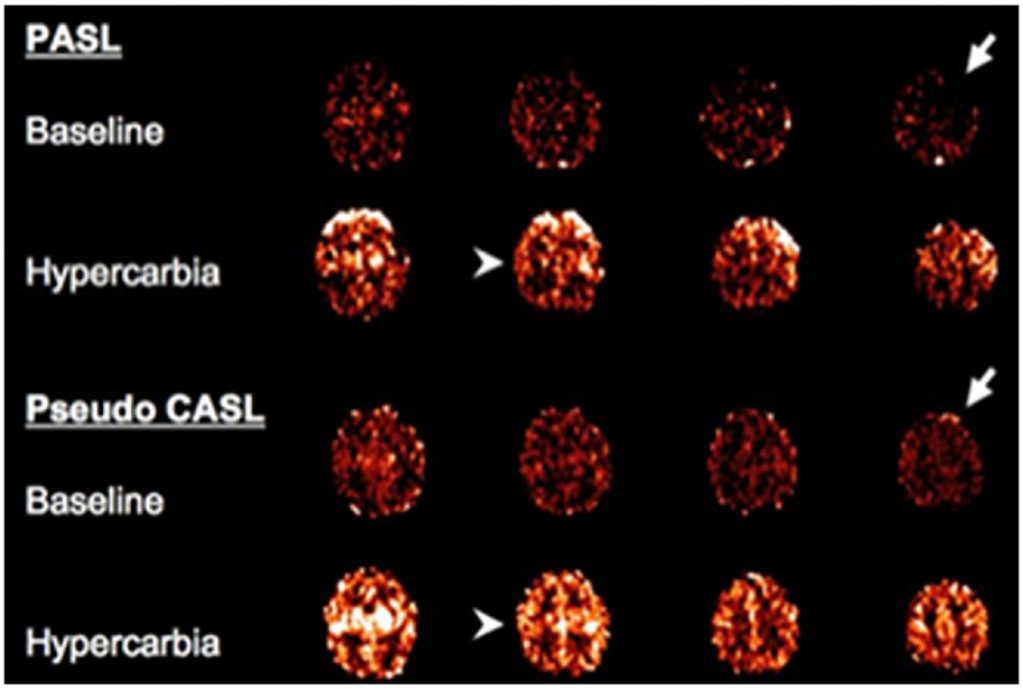

Figure 3.
A direct comparison of PASL (upper) and pseudo CASL (lower). Images were obtained sequentially in a single patient both at rest (baseline) and hypercarbia. The 2 right arrows demonstrate increased negative pixels on PASL imaging in the left frontal cortex. The arrowheads on the left demonstrate improved anatomic resolution in the central sulcus. (Color version of figure is available online.)

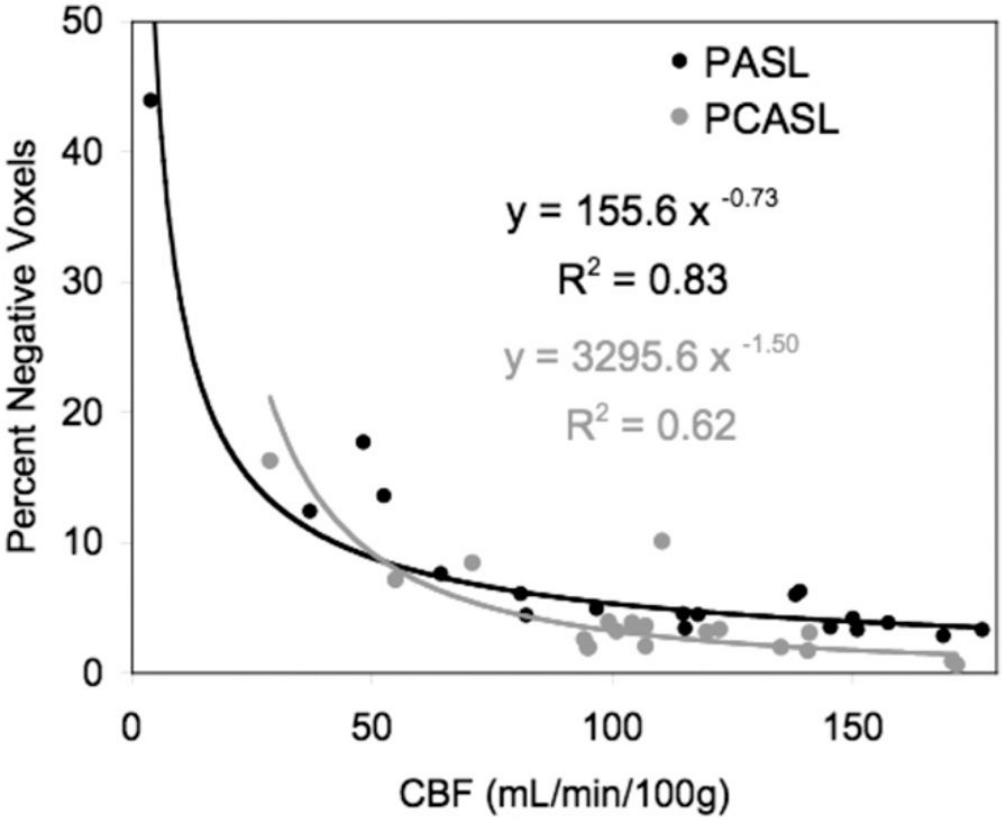

Figure 4.
Direct comparison of PCASL and PASL perfusion magnetic resonance imaging (MRI) in a cohort of infants and children with congenital heart disease. With increased values of cerebral blood flow (CBF), the percentage of negative voxels is reduced. PCASL offers an improvement in SNR at low blood flow values.

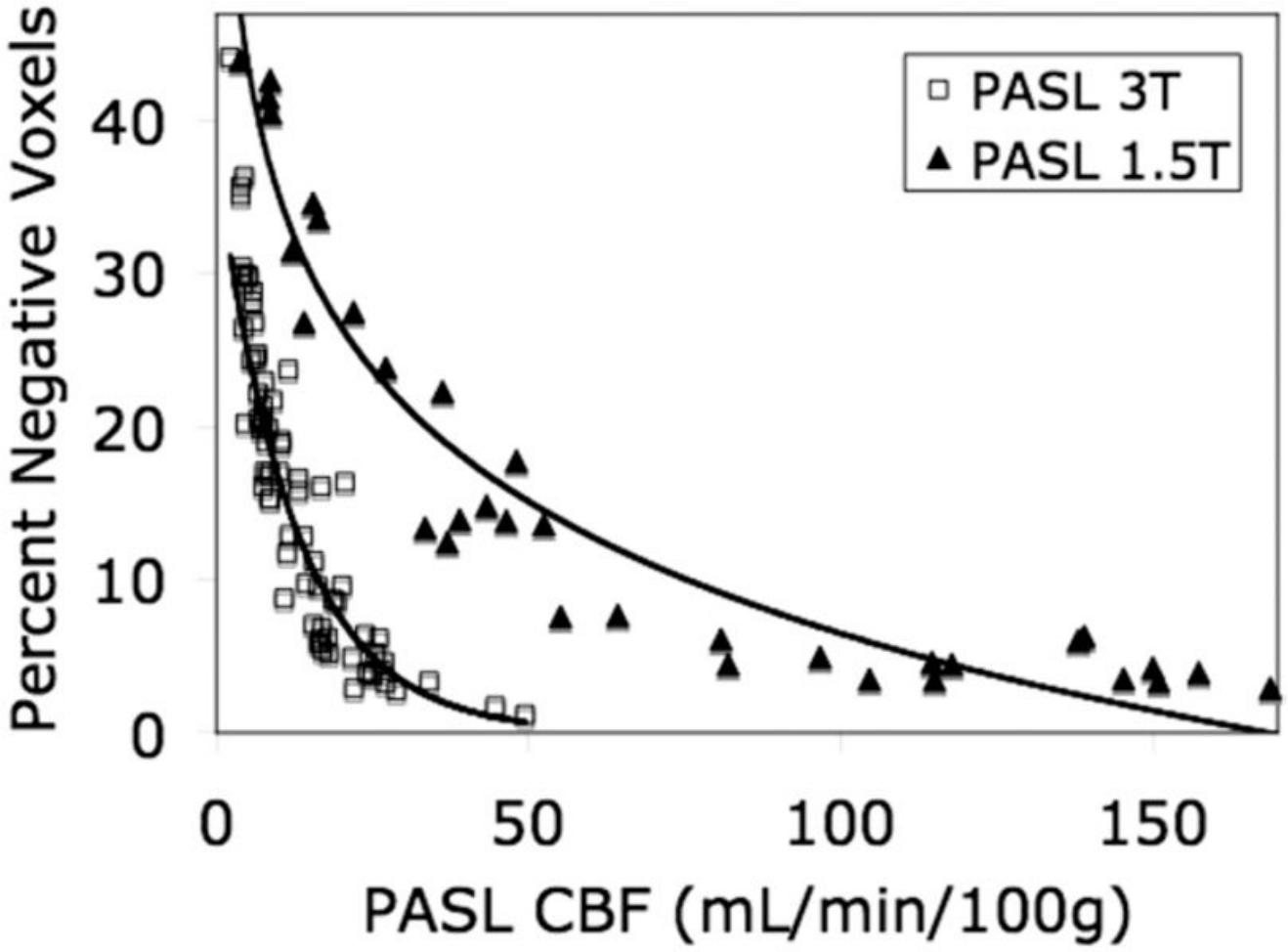

Figure 5.
Comparison of PASL perfusion MRI at 1.5 T (closed triangles) and 3 T (open squares) along with the best fit lines to both sets of data. Patients studied on the 3 T were all full-term infants with congenital heart defects, imaged before surgery in the first week of life.

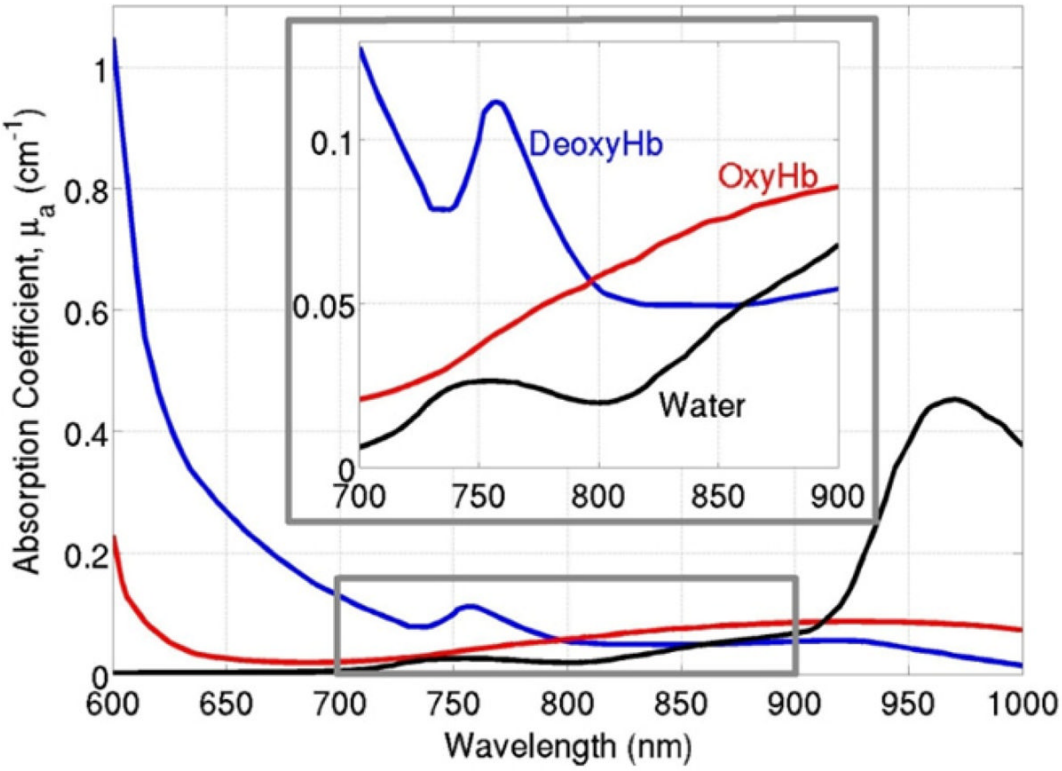

Figure 6.
A sample absorption spectrum of oxyhemoglobin, deoxyhemoglobin, and water in tissue. A spectral "window" exists in the near-infrared range (highlighted in the gray box and enlarged above), so that scattering, rather than absorption, dominates photon propagation. (Color version of figure is available online.)

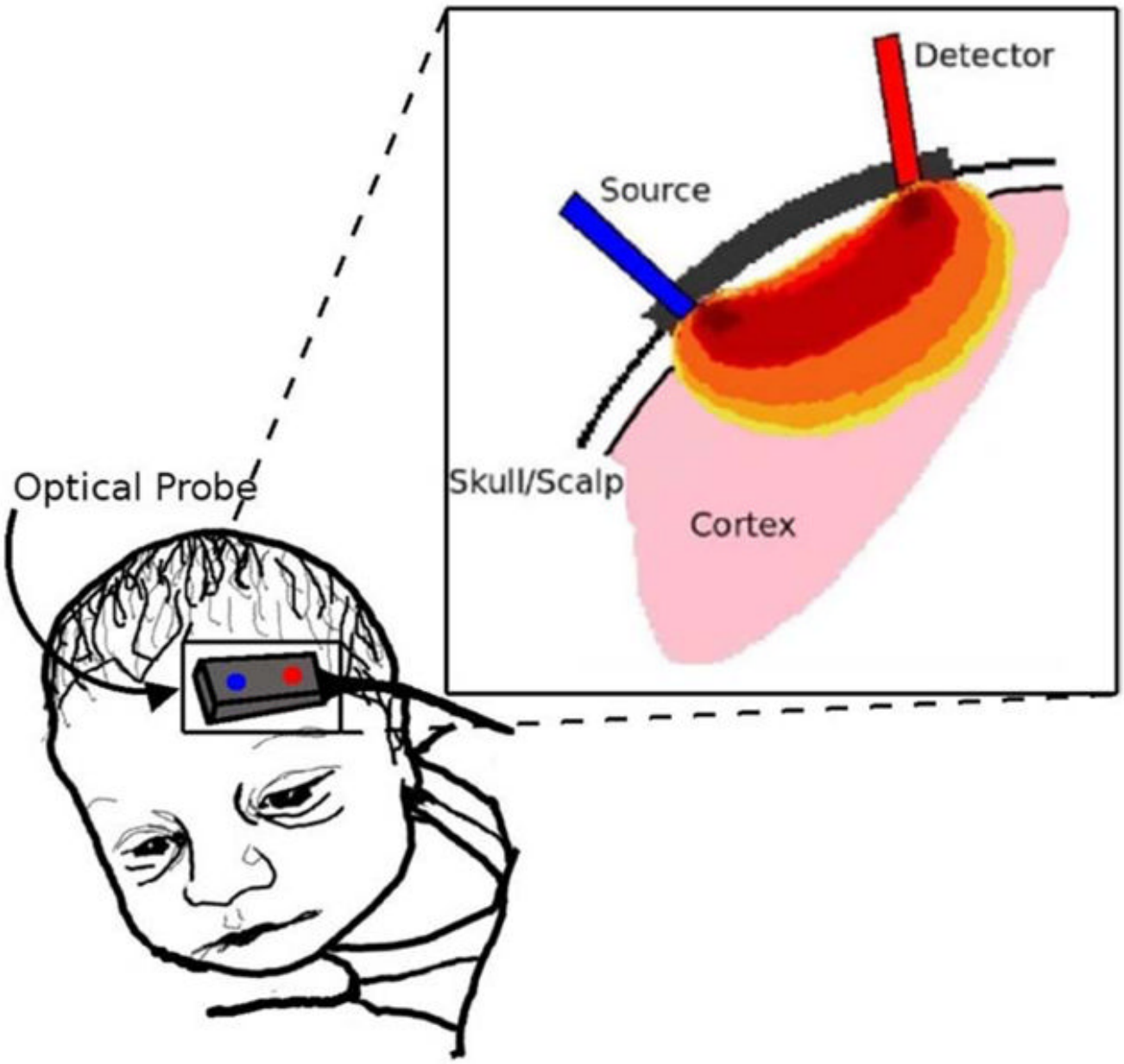

Figure 7.
Depiction of photon propagation through brain tissue. Light that reaches the detector is most likely affected by tissue in the darkest red region, while regions in orange or yellow have less effect on the photons' journey. The depth of photon penetration is highly dependent on source-detector separation. Larger separations lead to deeper penetration. (Color version of figure is available online.)

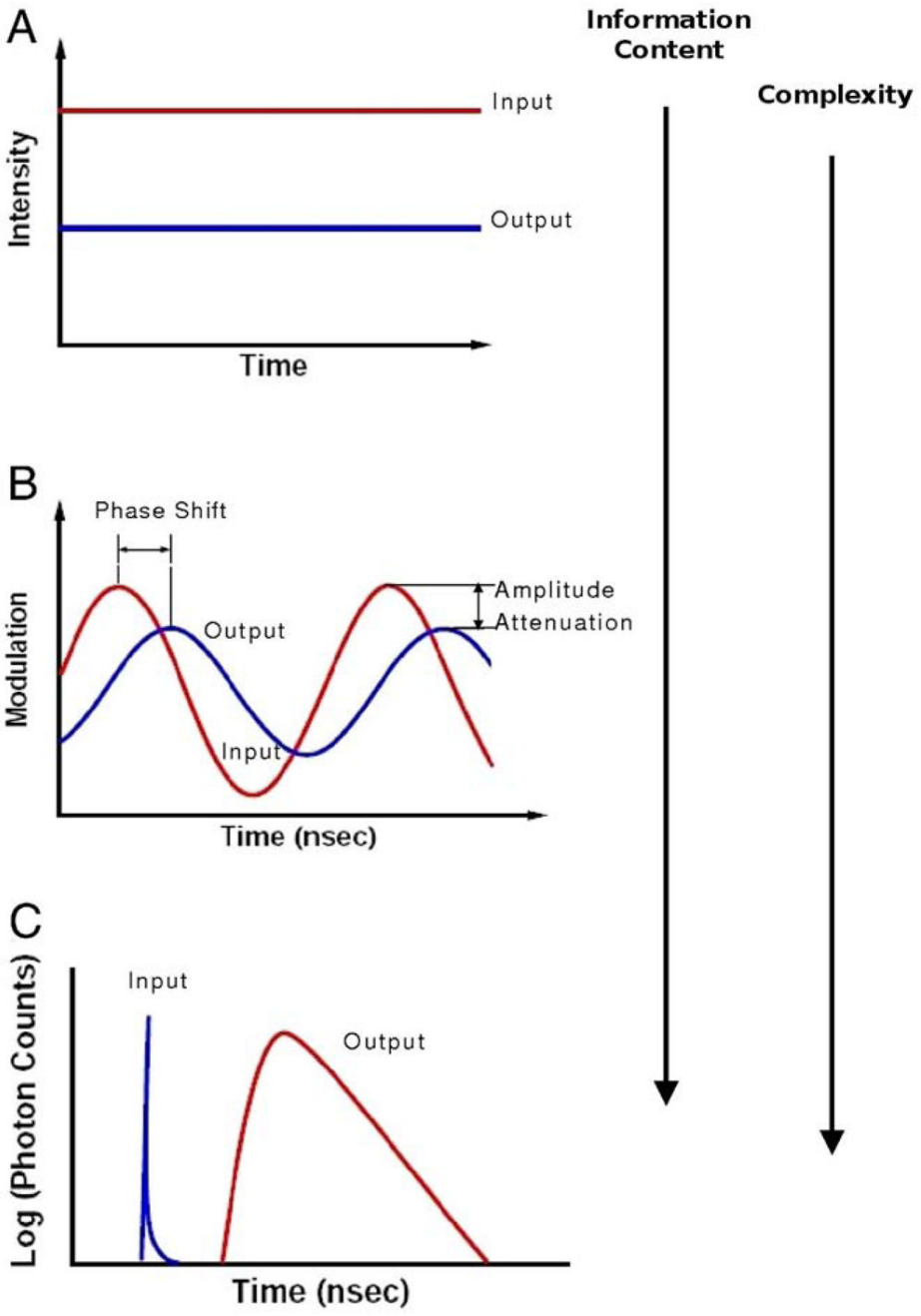

Figure 8.

Graphical depiction of the 3 types of near infrared spectroscopy measurements: (A) Continuous wave, (B) frequency domain, and (C) time resolved. The arrows on the right side of the figure indicate the increasing data and instrumentation complexity which accompany these techniques. (Color version of figure is available online.)

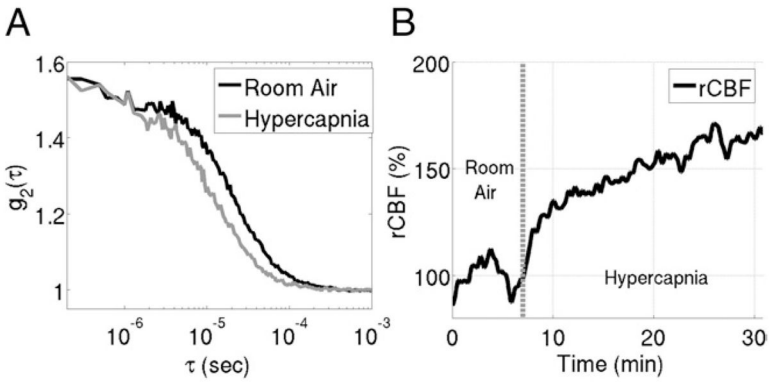

Figure 9.

(A) sample autocorrelation curve measured with diffuse correlation spectroscopy on a neonate with hypoplastic left heart syndrome. The "baseline" curve, taken on the patient's forehead during room air inhalation, decays slower than the hypercapnia curve taken while the patient inhaled a CO_2 gas mixture. The increase in the decay rate during hypercapnia indicates an increase in CBF compared with the resting baseline period. (B) Trace of relative change in cerebral blood flow (rCBF) during this hypercapnia experiment extracted from autocorrelation curves measured every 3 seconds.